Comprehensive analysis of a mouse model of spontaneous uveoretinitis using single-cell RNA sequencing

Jacob S. Heng[a,b], Sean F. Hackett[c], Genevieve L. Stein-O'Brien[b,d], Briana L. Winer[b,d], John Williams[a,e], Loyal A. Goff[b,d], and Jeremy Nathans[a,b,c,e,1]

[a]Department of Molecular Biology and Genetics, Johns Hopkins University School of Medicine, Baltimore, MD 21205; [b]The Solomon H. Snyder Department of Neuroscience, Johns Hopkins University School of Medicine, Baltimore, MD 21205; [c]Wilmer Eye Institute, Johns Hopkins University School of Medicine, Baltimore, MD 21205; [d]McKusick-Nathans Institute of Genetic Medicine, Johns Hopkins University School of Medicine, Baltimore, MD 21205; and [e]Howard Hughes Medical Institute, Johns Hopkins University School of Medicine, Baltimore, MD 21205

Contributed by Jeremy Nathans, October 29, 2019 (sent for review September 9, 2019; reviewed by Marie E. Burns and Douglas Vollrath)

Autoimmune uveoretinitis is a significant cause of visual loss, and mouse models offer unique opportunities to study its disease mechanisms. *Aire*$^{-/-}$ mice fail to express self-antigens in the thymus, exhibit reduced central tolerance, and develop a spontaneous, chronic, and progressive uveoretinitis. Using single-cell RNA sequencing (scRNA-seq), we characterized wild-type and *Aire*$^{-/-}$ retinas to define, in a comprehensive and unbiased manner, the cell populations and gene expression patterns associated with disease. Based on scRNA-seq, immunostaining, and in situ hybridization, we infer that 1) the dominant effector response in *Aire*$^{-/-}$ retinas is Th1-driven, 2) a subset of monocytes convert to either a macrophage/microglia state or a dendritic cell state, 3) the development of tertiary lymphoid structures constitutes part of the *Aire*$^{-/-}$ retinal phenotype, 4) all major resident retinal cell types respond to interferon gamma (IFNG) by changing their patterns of gene expression, and 5) Muller glia up-regulate specific genes in response to IFN gamma and may act as antigen-presenting cells.

Aire knockout | mouse model | ocular immunology | single-cell RNAseq | autoimmune uveitis

Noninfectious posterior uveitis, an autoimmune and/or autoinflammatory disease of the pars plana of the ciliary body, vitreous, choroid, and retina, affects ~0.01% of the population (1) and is estimated to be the fourth leading cause of severe vision loss in the industrialized world (2). When the disease encompasses the retina, it is often associated with autoreactivity to retinal antigens such as photoreceptor Arrestin and Interphotoreceptor Retinol Binding Protein (IRBP), and this is referred to as uveoretinitis (3).

Mouse models of autoimmune uveoretinitis offer unique opportunities to study the mechanisms of disease pathogenesis. The most widely used and best-characterized mouse model is referred to as experimental autoimmune uveitis/uveoretinitis (EAU) (4, 5). In the original EAU model, uveoretinitis is initiated by immunizing with a retinal antigen—typically IRBP or a peptide derived from IRBP—that has been emulsified in complete Freund's adjuvant (CFA). One limitation of this EAU model is the use of mineral oil supplemented with heat-killed mycobacteria, the active ingredient in CFA, which causes nonphysiological stimulation of the innate immune response. Inflammation is further enhanced by injection of pertussis toxin, which is required for efficient disease production in most rodent strains. These treatments may alter the adaptive immune response, which is considered to be the central driver of uveoretinitis. In contrast, adjuvant-free models of uveitis rely on genetic backgrounds that increase the number of auto-reactive T cells and have a more protracted clinical course relative to the original EAU model (6).

Loss of central tolerance to retinal antigens has been shown to mediate the development of spontaneous uveoretinitis (7). Many retinal antigens, including IRBP, are expressed in the thymus under the control of the Autoimmune Regulator (AIRE) transcription factor (8), and the susceptibility of mouse strains to EAU has been shown to correlate inversely with the amount of IRBP expressed in the thymus (9). *Aire* knockout (*Aire*$^{-/-}$) mice develop a spontaneous and chronic-progressive uveoretinitis as part of a multiorgan autoimmune phenotype, and, therefore, *Aire*$^{-/-}$ mice represent an adjuvant-free model of uveoretinitis secondary to a loss of central tolerance to retinal antigens (10–12). The *Aire*$^{-/-}$ mouse phenotype resembles autoimmune polyendocrinopathy-candidiasis-ectodermal dystrophy (13, 14), a human condition caused by loss-of-function mutations in the human *AIRE* gene. At present, the *Aire*$^{-/-}$ uveoretinitis model is relatively unexplored in terms of the immune cell types involved, the dominant effector response, and the response of resident retinal cells.

Droplet-based single-cell RNA sequencing (scRNA-seq) has emerged as a powerful and unbiased method for characterizing cell types in complex tissues in both normal and disease contexts (15, 16). Thus far, scRNA-seq has not yet been used to characterize uveoretinitis. To define the full range of cell types and

Significance

Autoimmune inflammatory diseases of the retina represent a major source of vision loss worldwide. Single-cell RNA sequencing has been used as a comprehensive and unbiased approach to investigate cell types and gene expression patterns in the retinas of a mouse model of spontaneous, chronic, and progressive autoimmune uveoretinitis. This work defines the dominant immune effector cell types involved, reveals the development of tertiary lymphoid structures within the diseased retina, characterizes the conversion of monocytes to a macrophage/microglia state or a dendritic cell state, shows that essentially all resident retinal cell types respond to interferon gamma as part of the disease process, and suggests that Muller glia may act as antigen-presenting cells.

Author contributions: J.S.H., L.A.G., and J.N. designed research; J.S.H., S.F.H., B.L.W., and J.W. performed research; J.S.H., G.L.S.-O., L.A.G., and J.N. analyzed data; and J.S.H. and J.N. wrote the paper.

Reviewers: M.E.B., University of California, Davis; and D.V., Stanford University School of Medicine.

The authors declare no competing interest.

Data deposition: scRNA-seq data reported in this paper have been deposited in the National Center for Biotechnology Information Gene Expression Omnibus database (accession nos. GSE132229 and GSM3854512–GSM3854519). The annotated datasets can be viewed at https://jacobheng.shinyapps.io/uveoretinitis/ and http://loom.gofflab.org. Supplementary code for processing and visualizing the scRNA-seq data can be found in an R package, cellwrangler, available at https://github.com/jacobheng/cellwrangler.

[1]To whom correspondence may be addressed. Email: jnathans@jhmi.edu.

This article contains supporting information online at https://www.pnas.org/lookup/suppl/doi:10.1073/pnas.1915571116/-/DCSupplemental.

First published December 16, 2019.

cellular responses in a mouse model of uveoretinitis, we have characterized the neural retinas of *Aire*$^{-/-}$ mice on a C57BL/6J background using scRNA-seq, with additional analyses using immunostaining and in situ hybridization (ISH).

Results

scRNA-seq Reveals a Diverse Immune Cell Infiltrate in Uveoretinitis. To characterize uveoretinitis in *Aire*$^{-/-}$ mice on a C57BL/6J background, we performed retinal imaging on mice between 5 and 25 wk of age and graded disease severity according to the published EAU clinical grading scale (*SI Appendix*, Fig. S1*A*) (17). We used mice between 10 and 16 wk of age for scRNA-seq and mice between 8 and 25 wk of age for immunohistochemistry. As previously described (6), *Aire*$^{-/-}$ mice develop a chronic-progressive spontaneous uveoretinitis, as seen in the fundus images and fluorescein angiograms obtained from one *Aire*$^{-/-}$ mouse at 5 time points over 20 wk (*SI Appendix*, Fig. S1*B*). Fig. 1*A* shows representative images of retina cross-sections with their corresponding fundus images for each clinical grade. In general, there was progressive retinal thinning and an increase in the number of infiltrating CD45-positive leukocytes with higher disease grade, consistent with previous descriptions of *Aire*$^{-/-}$ eyes on a B10.RIII background (6). In a minority of mice, the uveoretinitis was largely limited to one eye (*SI Appendix*, Fig. S1*C*).

Using a droplet-based scRNA-seq platform (10× Genomics), we characterized 64,196 dissociated retinal cells from 8 samples (one neural retina per sample): 2 grade 2 *Aire*$^{-/-}$ mice (16,884 cells), 2 grade 3 *Aire*$^{-/-}$ mice (12,640 cells), and their wild-type (WT) littermate controls (34,672 cells) (Fig. 1*B*). The mean number of genes detected was 928 per cell (median: 584; interquartile range: 383 to 1,289). To control for sex effects, only female mice were studied. By principal component analysis, the samples were clearly segregated by disease grade (*SI Appendix*, Fig. S1*D*). On a Uniform Manifold Approximation and Projection (UMAP) (18) plot, the single-cell transcriptomes segregated predominantly by cell type (Fig. 1*C*), based on known markers for the 12 major retinal cell types (*SI Appendix*, Table S1), rather than by disease grade or batch (*SI Appendix*, Fig. S1*E*). (In this UMAP plot, microglia constitute a subset of the cell clusters labeled "Immune cells.") A total of 1,266 presumed multiplets were excluded from subsequent analyses.

In *Aire*$^{-/-}$ retinas, scRNA-seq revealed multiple immune cell types. When visualized on a separate UMAP plot, these cells formed distinct clusters representing microglia, cells of monocyte lineage, T and Natural Killer (NK) cells, B cells, and plasma cells (Fig. 1*D* and *SI Appendix*, Table S2). In WT retinas, a small number of monocyte-derived cells that are transcriptionally distinct from microglia were present (Fig. 1 *E*, *Left*), but B cells, T and NK cells, and plasma cells were not detected. The absence or near-absence of lymphoid cells in WT retinas may be a feature of ocular immune privilege (5). In *Aire*$^{-/-}$ retinas, there were many more nonresident immune cells, and there was a preponderance of T and NK cells and monocyte-derived cells, accompanied by a smaller number of B cells and plasma cells (Fig. 1 *E*, *Right*). The proportion of B cells and plasma cells increased with disease severity [χ^2 = 37.855, degree of freedom (df) = 6, *P* value = 1.199 × 10^{-6}].

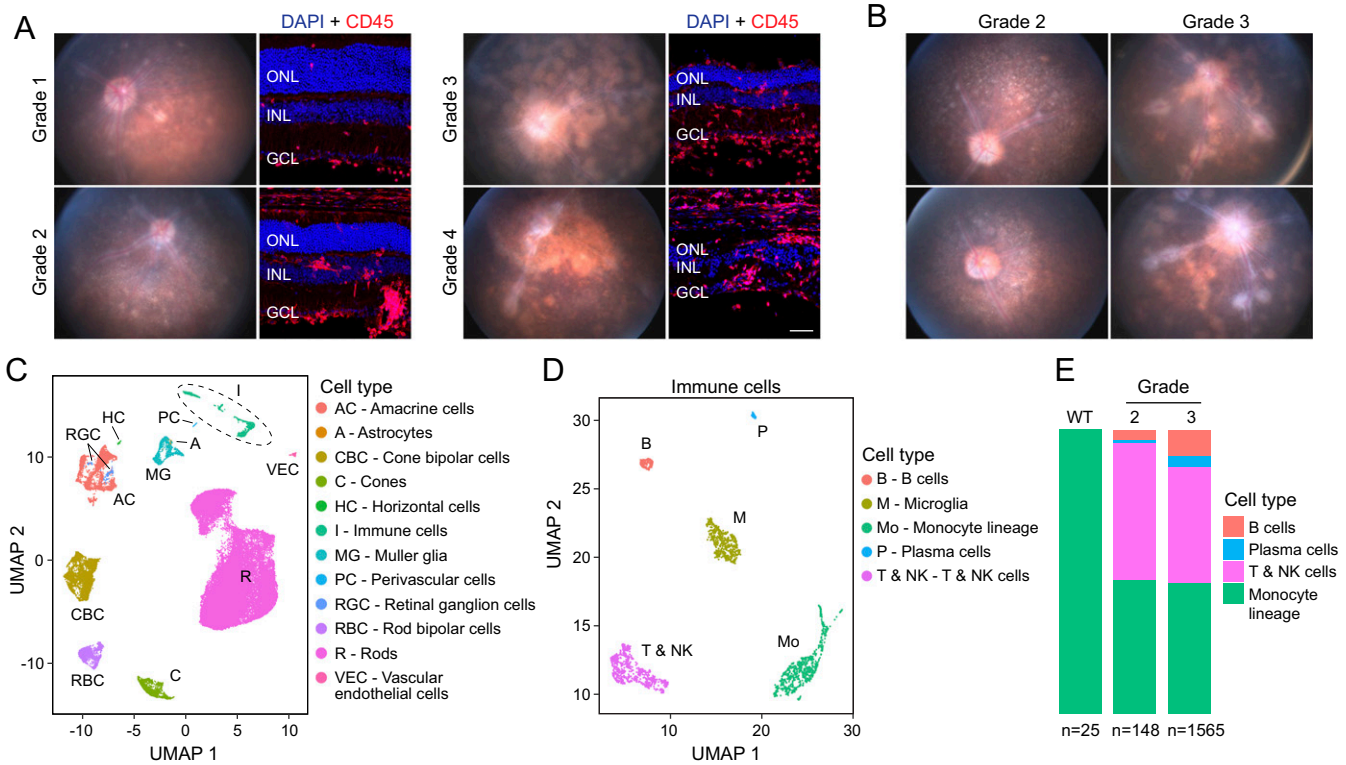

Fig. 1. Characterization and scRNA-seq analysis of *Aire*$^{-/-}$ retinas. (*A*) *Aire*$^{-/-}$ retina fundus photographs (*Left*) and immunostaining of the corresponding cross-sections (*Right*) showing leukocytes (CD45; red) and nuclei (DAPI; blue). Representative examples of grade 1 to grade 4 uveoretinitis are shown. In this and other retina cross-sections, the following abbreviations are used: ONL, outer nuclear layer; INL, inner nuclear layer; GCL, ganglion cell layer. (Scale bar, 50 μm.) (*B*) Fundus photographs of 4 *Aire*$^{-/-}$ retinas used for scRNA-seq. (*C*) UMAP plot showing different cell-type clusters in a merged dataset from duplicate samples of *Aire*$^{-/-}$ retinas (shown in *B*) and age- and sex-matched WT control retinas. (*D*) UMAP plot of immune cells in the merged dataset. (*E*) Stacked bar plots showing the proportions of nonmicroglial immune cell types in scRNA-seq datasets from *Aire*$^{-/-}$ and WT retinas. The numbers of immune cells in each dataset are indicated below.

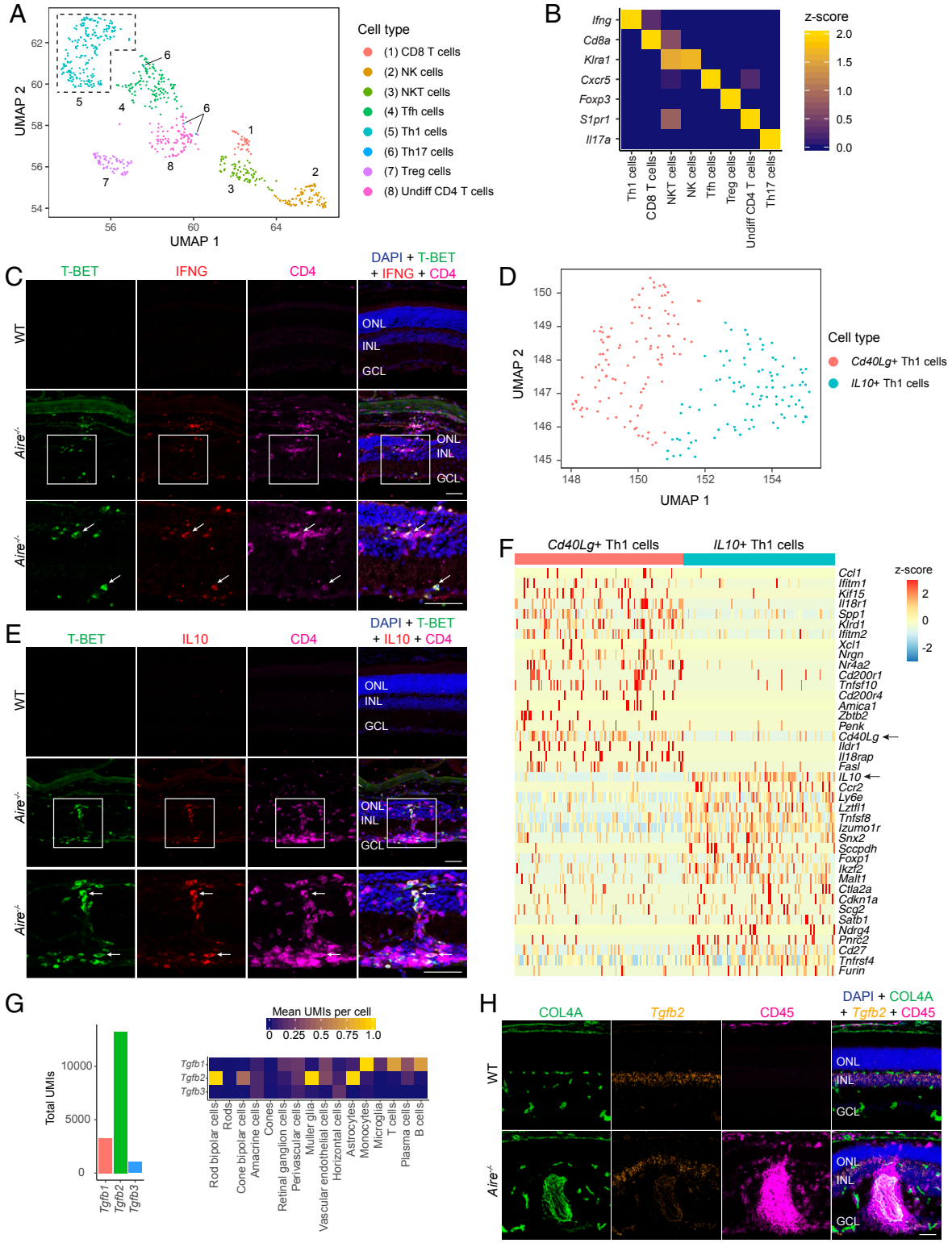

Fig. 2. Analysis of T cell diversity in *Aire*$^{-/-}$ retinas. (*A*) UMAP plot of *Cd3*-expressing cells from *Aire*$^{-/-}$ retinas showing different T cell and NK cell subtypes. (*B*) Heatmap showing, for each T and NK cell subtype (horizontal axis), the scaled mean unique molecular identifiers (UMIs) of transcripts for known cell-type markers (vertical axis). (*C*) Immunostaining of cross-sections of WT vs. *Aire*$^{-/-}$ retinas showing T-BET (green), IFNG (red), CD4 (magenta), and nuclei (DAPI; blue). T-BET+ IFNG+ CD4+ Th1 cells are indicated by arrows. In this and other figures, the regions in the square *Insets* are enlarged below. (*D*) UMAP replotting of Th1 cells from the UMAP plot in *A* enclosed in dashed lines showing 2 distinct clusters of Th1 cells: a *Cd40-ligand* (*Cd40Lg*)–positive cluster and an *IL10*-positive cluster (*SI Appendix*, Fig. S2*B*). (*E*) Immunostaining of cross-sections of WT vs. *Aire*$^{-/-}$ retinas showing T-BET (green), IL10 (red), CD4 (magenta), and nuclei (DAPI; blue). T-BET+ IL10+ CD4+ Tfh cells are indicated by arrows. (*F*) Heatmap showing 40 genes that are differentially expressed between the 2 Th1 clusters. (*G*, *Left*) Bar plots showing total UMIs for *Tgfb1*, *Tgfb2*, and *Tgfb3*. (*G*, *Right*) Heatmap showing mean expression per cell of *Tgfb1*, *Tgfb2*, and *Tgfb3* for each cell type. (*H*) Retinal cross-sections showing fluorescent ISH for *Tgfb2* (orange) and immunostaining for COL4A (green) and CD45 (magenta); nuclei are marked by DAPI (blue). (Scale bars in *C*, *E*, and *H*, 50 μm.)

We note the lack of significant expression of *Aire* transcripts in resident retinal cells in the WT mouse retina, implying that the phenotype associated with *Aire* loss of function reflects *Aire* expression in nonretinal cells, presumably medullary thymic epithelial cells (8, 11, 12). In a previous study, transfer of thymi from $Aire^{-/-}$ mice into *Aire*-sufficient athymic mice was sufficient to induce autoantibodies to eye antigens (8).

Analysis of T Cell Diversity Reveals Th1 Cells as the Main Effector T Cells. Since experimental uveoretinitis has been characterized as a T cell-driven disease (5), we analyzed the cluster of cells that express *Cd3e* or *Klra1* transcripts or both—representing T cells and NK cells—by first embedding these cells on a separate UMAP plot (Fig. 2*A*). By classifying cells according to known markers (Fig. 2*B* and *SI Appendix*, Table S2), we identified the following 6 classes: Th1 cells (*T-bet*+, *Ifng*+, *Cxcr6*+, *Cd4*+, *Cd8a*−, *Klra1*−), *Cd8a*+ T cells (*Cd8a*+, *Cd4*-, *Klra1*−), T follicular helper (Tfh) cells (*Bcl6*+, *Cxcr5*+, *Cd4*+, *Cd8a*−), regulatory T (Treg) cells (*Foxp3*+, *Cd4*+, *Il10*+), NK cells (*Klra1*+, *Cd3e*−, *Cd4*−, *Cd8a*−), and NK T cells (*Klra1*+, *Cd3e*+, *Cd8a*+). We also found a population of apparently undifferentiated *Cd4*+ T cells that were enriched for *S1pr1* but did not express any of the classical effector T cell markers (*S1pr1*+, *Cd3*+, *Cd4*+, *Cd8a*−). Only 3 of 714 T and NK cells in $Aire^{-/-}$ retinas were classified as Th17 cells, as defined by *IL17a* expression (Fig. 2 *A* and *B*). These presumed Th17 cells do not form a distinct cluster on the UMAP plot, but this could reflect a combination of the small number of cells and/or variation in their gene expression profiles.

The classification of the different T cell populations revealed Th1 cells as the predominant class of T helper cells in $Aire^{-/-}$ retinas. Direct quantification of Th1 and Th17 markers in *Cd4*+ T cells revealed a predominance of Th1 markers in both grade 2 and grade 3 disease (*SI Appendix*, Fig. S2*A*). Immunostaining of $Aire^{-/-}$ retinas for T-BET, interferon gamma (IFNG), and CD4 verified the presence of Th1 cells, which express all of these markers (Fig. 2*C*). The predominance of Th1 cells as effector T cells in the $Aire^{-/-}$ retina is consistent with previous reports that the main effector response in nonocular $Aire^{-/-}$ tissues is Th1 dominant (19). Closer examination of the scRNA-seq data derived from the Th1 population revealed 2 distinct clusters—one that is *IL10*+ (Interleukin-10+) and another that is *Cd40lg*+ (*Cd40* ligand+) (Fig. 2*D*). These clusters appear to represent the previously described activated (*Cd40lg*+) and self-regulatory (*Il10*+) states, respectively (20). These 2 states were correlated with the differential expression of multiple genes (Fig. 2*F*) that may underlie the dynamics of Th1 cell self-regulation. Notably, both of these Th1 subpopulations express the IFN gamma (*Ifng*) gene and the Th1 markers *Cxcr6* and *Tbx21*, the latter coding for T-BET (*SI Appendix*, Fig. S2*B*). The *IL10*-expressing Th1 cells do not express *Foxp3*, indicating that they are not regulatory T cells (*SI Appendix*, Fig. S2*B*). Fig. 2*E* shows accumulation of IL10 in a subset of T-BET+ and CD4+ T cells in the $Aire^{-/-}$ retina.

Th1 cells are sensitive to transforming growth factor-beta (TGF-β), which has been shown to promote either an effector state or a self-regulatory state, depending on the context (21). Promoting a self-regulatory state associated with induction of *Il10* appears to be the predominant response for mature Th1 cells, as seen, for example, in a mouse model of experimental autoimmune encephalitis (22). Our scRNA-seq data show that *Tgfb2* is the principal TGF-β family member expressed in both WT and $Aire^{-/-}$ retinas and that it is expressed by multiple retinal cell types, predominantly in the inner nuclear layer (INL) (Fig. 2*G*), which was confirmed by fluorescent ISH (Fig. 2*H*). There was no difference in the mean abundance of *Tgfb2* transcripts between WT and $Aire^{-/-}$ retinas (*SI Appendix*, Fig. S2 *C* and *D*). *Tgfb1* transcripts were present at a lower level and were detected principally in infiltrating immune cells, especially in cells of the monocyte lineage.

Tfh Cells and the Formation of Tertiary Lymphoid Structures. The cluster of *Bcl6*+, *Cxcr5*+, *Cd4*+, and *Cd8a*− cells observed with scRNA-seq of $Aire^{-/-}$ retinas match the profile of Tfh cells (23, 24). This raises the possibility that tertiary lymphoid structures (TLSs) could have formed within $Aire^{-/-}$ retinas, a phenomenon that has been reported in the R161H mouse line, a mouse model of spontaneous uveoretinitis that is driven by transgenic expression of a T cell receptor (TCR) that recognizes IRBP (25).

By immunostaining of $Aire^{-/-}$ retinas, we observed aggregates of CD4+ T cells, CD8+ T cells, and CD19+ B cells (Fig. 3*A*). There appeared to be a predominance of CD4+ T cells over CD8+ T cells, as reflected in the scRNA-seq data, where 61.3% ($\chi^2 = 8.1667$, df = 1, P value = 4.27×10^{-3}) and 76.3% ($\chi^2 = 255.12$, df = 1, P value < 2.2×10^{-16}) of all T cells detected in grade 2 and grade 3 disease, respectively, were *Cd4*+ T cells (*SI Appendix*, Fig. S2*E*). To assess whether these cell aggregates might resemble TLSs, we assessed markers indicative of TLSs. This analysis revealed the close proximity of BCL6+;CD4+ presumptive Tfh cells and CD19+ B cells in these cell aggregates (Fig. 3*B*). We also detected the classical germinal center marker Peripheral Lymph Node Addressin (PNAd) in close proximity to aggregates of CD19+ B cells and CD4+ T cells (Fig. 3*C*). PNAd is a glycoprotein that promotes the homing of T and B cells to TLSs and is a marker for high endothelial venules (HEVs), which are postcapillary venous structures important for lymphocyte homing and trafficking (26). We found PNAd+ blood vessels in close proximity to the cell aggregates (Fig. 3*C*). The aggregates also exhibited close apposition of CCR7+;CD4+ T cells and CCR7+ antigen-presenting cells (APCs), characterized by the expression of the major histocompatibility complex (MHC) class II proteins and visualized by immunostaining with an antibody directed against I-A and I-E MHC class II proteins (Fig. 3*D*). CCR7 has been shown to be important for organizing the T cell zone in lymph nodes and is necessary for the formation of TLSs (27). Finally, the detection of phosphorylated ZAP70 in CD4+ T cells and the presence of the costimulatory molecule CD80 indicate that TCR activation was occurring in these presumed TLSs (Fig. 3*E*). Consistent with CD4+ T cell activation and signaling, the TLSs also contained CD19+, SDC1+ plasmablasts, and CD19− and SDC1+ plasma cells (Fig. 3*F*).

Monocyte Transitional States: Microglia-Like Macrophages and Dendritic Cells. As shown in Fig. 1 *C* and *D*, retinal microglia and cells of the monocyte lineage form transcriptionally distinct clusters when visualized on a UMAP plot. Based on recent scRNA-seq studies of microglia and macrophages in the brain and retina (28–30), we were able to further resolve the cells of the monocyte lineage into monocytes, monocyte-derived macrophages (mo-MΦs), monocyte-derived dendritic cells (mo-DCs), replicating monocytes, perivascular macrophages, and plasmacytoid dendritic cells (Fig. 4*A*). Each of these populations of cells expressed distinct markers (*SI Appendix*, Fig. S3*A*). Two populations of cells, termed macrophage-committed monocytes (MΦ-committed Mo) and dendritic cell-committed monocytes (DC-committed Mo), expressed macrophage and dendritic markers, respectively, in addition to monocyte markers (*SI Appendix*, Fig. S3*B*).

Since monocytes, MΦ-committed Mo, mo-MΦs, DC-committed Mo, and mo-DCs formed a continuum on a UMAP plot from $Aire^{-/-}$ retinas (Fig. 4*A*), we constructed a cell trajectory map for these cell types. Starting with *Ccr2*+ monocytes, this trajectory bifurcates into mo-MΦs (branch 1) and mo-DCs (branch 2) (Fig. 4*B*). The cell trajectory analysis shows that, as monocytes progress toward MΦs, they reduce expression of the monocyte markers *Anxa8*, *Ly6c2*, and *Ccr2*, while increasing expression of macrophage

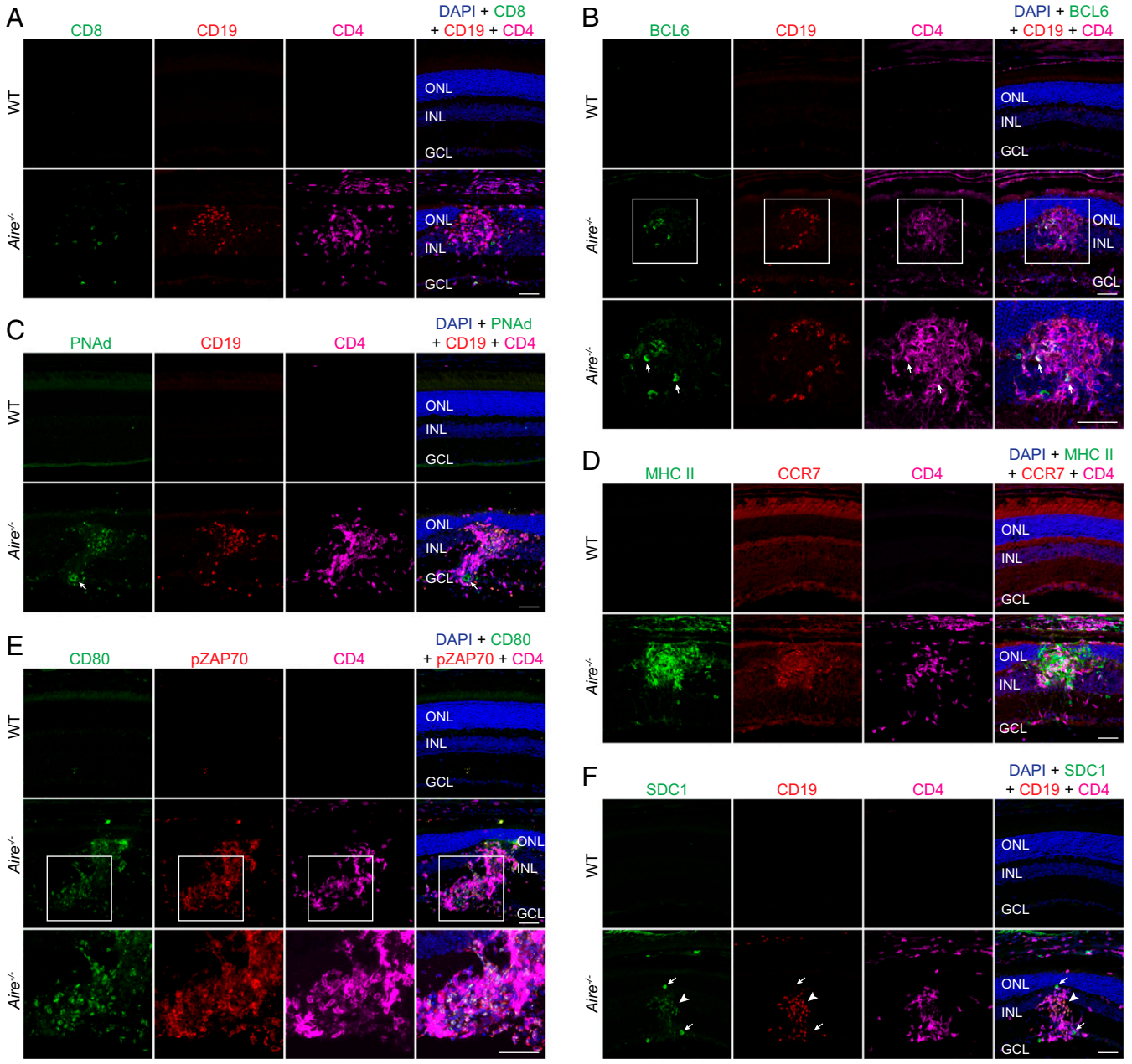

Fig. 3. Presence of tertiary lymphoid structures in *Aire*$^{-/-}$ retinas. (*A–D*) Immunostaining of cross-sections of WT vs. *Aire*$^{-/-}$ retinas. (*A*) CD8 (green), CD19 (red), CD4 (magenta), and nuclei (DAPI; blue). (*B*) BCL6 (green), CD19 (red), CD4 (magenta), and nuclei (DAPI; blue). BCL6+CD4+ cells are indicated by arrows. (*C*) PNAd (green), CD19 (red), CD4 (magenta), and nuclei (DAPI; blue). A PNAd+ vessel resembling an HEV is indicated by the arrows. (*D*) MHC class II (I-A and I-E; green), CCR7 (red), CD4 (magenta), and nuclei (DAPI; blue). (*E*) CD80 (green), pZAP70 (red), CD4 (magenta), and nuclei (DAPI; blue). (*F*) SDC1 (green), CD19 (red), CD4 (magenta), and nuclei (DAPI; blue). CD19− SDC1+ plasma cells are indicated by arrows; a CD19+ SDC1+ plasmablast is indicated by the arrowheads. (Scale bars in *A–F*, 50 μm.)

markers, including *Trem2* and *Hexb* (Fig. 4*C*). Interestingly, the mo-MΦs also increase expression of classical microglial markers such as *Tmem119* and *P2ry12*. This observation is consistent with the findings of a previous study indicating that bone-marrow–derived monocytes can migrate into both the normal and the injured retina to assume a microglia-like ramified morphology with expression of microglial markers (31). Similarly, as monocytes progress toward mo-DCs, they increase expression of DC markers, including *Clec9a* and *Zbtb46* (Fig. 4*C*). Fig. 4*D* illustrates, on a cell-by-cell basis, the changing patterns of expression for 5 markers: *Cd14*, which is enriched in monocytes, MΦ-committed Mo, and mo-MΦs; *Mrc1*, which codes for CD206 and is expressed in monocytes and MΦ-committed Mo; *P2ry12*, which is enriched in mo-MΦs (and microglia); *Smad7*, which is a marker of TGF-β signaling and is up-regulated as monocytes convert to mo-MΦs and to mo-DCs; and *Zbtb46*, a marker of dendritic cells, which is enriched in mo-DCs.

A recent study has shown that, in mouse models of photoreceptor degeneration, resident microglia migrate to the subretinal space and adhere to the apical retinal pigment epithelium (RPE), whereas infiltrating monocytes and mo-MΦs remain in the neural retina (29). In a similar fashion, immunostaining of *Aire*$^{-/-}$ retinas showed P2RY12+;CD14+ mo-MΦs and IBA1+;MRC1+ MΦ-committed-Mo predominantly in the neural retina, with only occasional

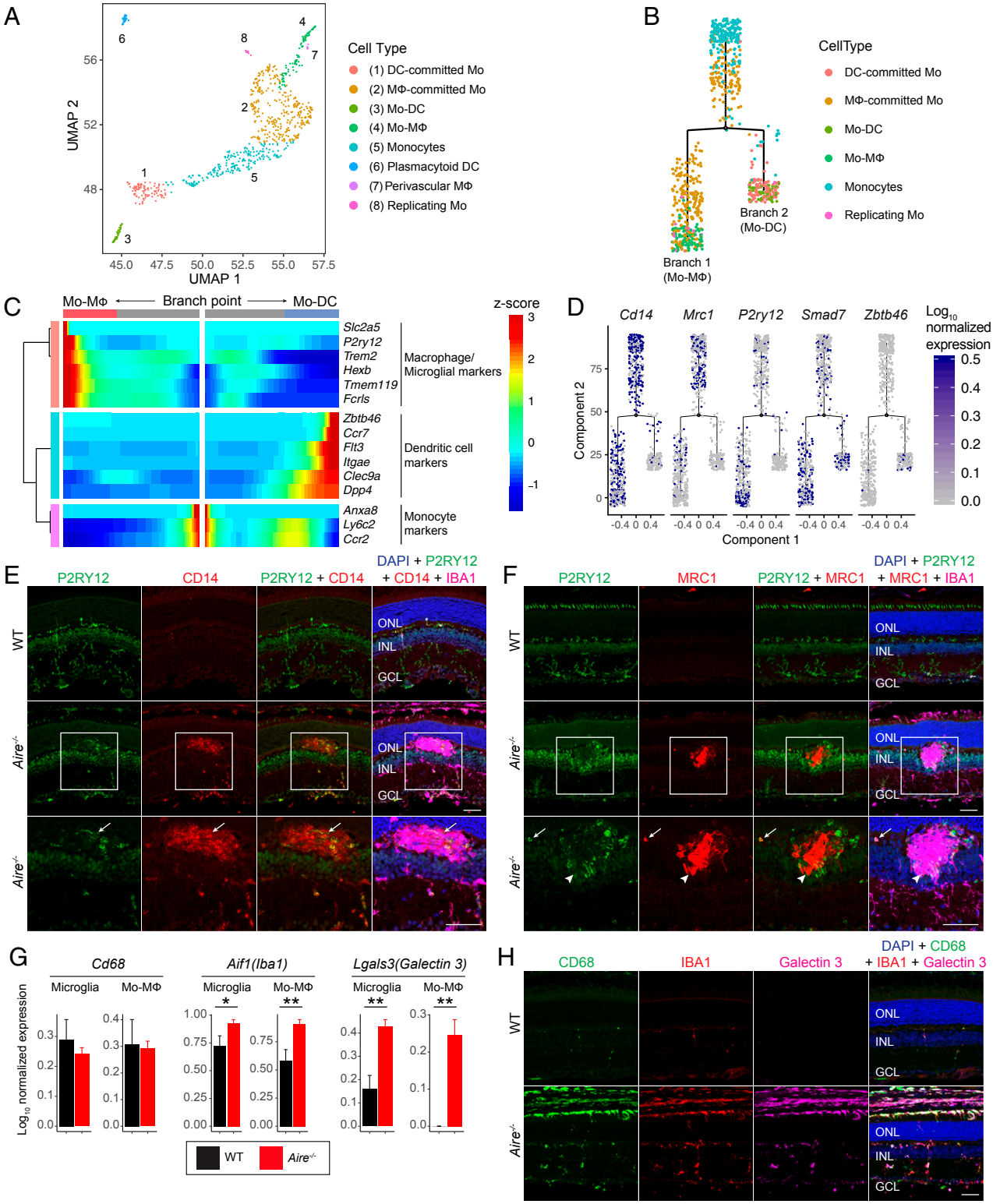

Fig. 4. Divergent fates of monocyte lineage cells in *Aire*$^{-/-}$ retinas. (*A*) UMAP plot from *Aire*$^{-/-}$ retinas showing different subtypes of monocyte lineage cells. (*B*) Cell trajectory of monocyte lineage cells showing a bifurcation into Mo-MΦs and Mo-DCs. (*C*) Heatmap showing branch expression analysis modeling of the branch point between Mo-MΦs (*Left*) and Mo-DCs (*Right*). (*D*) Expression of *Cd14*, *Mrc1*, *P2ry12*, *Smad7*, and *Zbtb46* along the cell trajectory shown in *B*. (*E*) Immunostaining of cross-sections of WT vs. *Aire*$^{-/-}$ retinas showing P2RY12 (green), CD14 (red), IBA1 (magenta), and nuclei (DAPI; blue). A P2RY12+ CD14+ cell is indicated by the arrows. (*F*) Immunostaining as in *E* for P2RY12 (green), MRC1 (red), IBA1 (magenta), and nuclei (DAPI; blue). Most IBA1+ P2RY12+ cells are MRC1− (indicated by arrowheads) with a minority being MRC1+ (indicated by arrows). (*G*) Barplots showing mean $\log_{10}$ normalized expression per cell for *Cd68*, *Aif1*, and *Lgals*. **P* value < 0.05 and ***P* value < 0.01. (*H*) Immunostaining as in *E* for CD68 (green), IBA1 (red), Galectin 3 (magenta), and nuclei (DAPI; blue). (Scale bars in *E*, *F*, and *H*, 50 μm.)

P2RY12+;CD14+ cells in the subretinal space (Fig. 4 *E* and *F*). Interestingly, colonization of the microglial niche by mo-MΦs has been shown to be TGF-β dependent in the brain and retina (32, 33).

In previous studies, it has been difficult to distinguish infiltrating mo-MΦs from resident microglia because the 2 cell types exhibit similar patterns of gene expression and undergo similar gene expression changes in response to disease (34). Therefore, we examined gene expression patterns and disease-associated changes in those patterns in mo-MΦs and resident microglia in *Aire*$^{-/-}$ retinas. Some genes, such as *Hexb* and *Trem2*, are expressed at similar levels in both mo-MΦs and resident microglia (*SI Appendix*, Fig. S4*A*). Other genes are more specific to one or the other population. In particular, we examined *Galectin-3* (*Lgals3*)

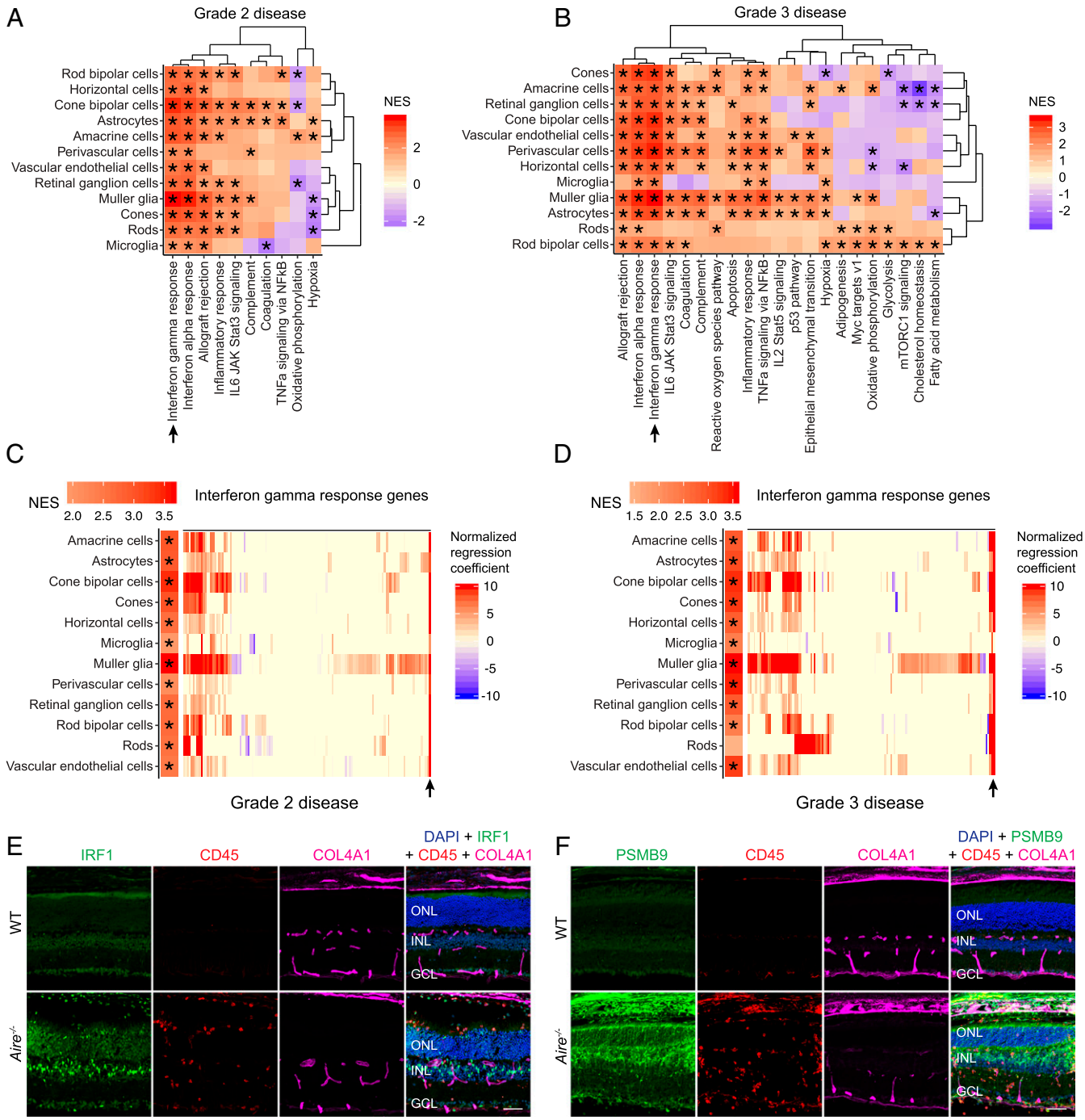

Fig. 5. IFN gamma response in resident cells in *Aire*$^{-/-}$ retinas. (*A* and *B*) Statistically significant MSigDB Hallmark pathways in 3 or more cell types in GSEA reveal pathways enriched in *Aire*$^{-/-}$ over WT retinas across multiple retinal cell types in grade 2 and grade 3 disease. *P value < 0.05. (*C* and *D*) Heatmaps showing GSEA for the IFN gamma response gene set in grade 2 (*A*) and grade 3 (*B*) *Aire*$^{-/-}$ retinas. (*Left*) Single column showing normalized enrichment score (NES) for each cell type. (*Right*) Heatmap showing normalized regression coefficients for each cell type (rows represent cell types; columns represent genes). (*E*) Immunostaining of cross-sections of WT vs. *Aire*$^{-/-}$ retinas showing IRF1 (green), CD45 (red), COL4A1 (magenta), and nuclei (DAPI; blue). (*F*) Immunostaining as in *E* for PSMB9 (green), CD45 (red), COL4A1 (magenta), and nuclei (DAPI; blue). (Scale bars in *E* and *F*, 50 μm.)

and *Cd68*, as these 2 genes are enriched and up-regulated in subretinal microglia in a light damage model (29). In *Aire*$^{-/-}$ retinas, *Lgals3* was up-regulated in both mo-MΦs and resident microglia (P value < 0.01 for both), but *Cd68* was unchanged (Fig. 4*G*). Interestingly, we observed increased immunostaining for both Galectin-3 and CD68 in IBAI+ cells in *Aire*$^{-/-}$ retinas (Fig. 4*H*), suggesting that CD68 may be regulated post-transcriptionally. Both Galectin-3 and CD68 were detected in IBAI+ cells in the neural retina and the subretinal space, in contrast to their predominant subretinal localization in a light damage model (29). Transcripts coding for IBA1 (*Aif1*), a commonly used marker for microglia and macrophages, were only modestly up-regulated (P value < 0.05 for microglia and P value < 0.01 for mo-MΦs) (Fig. 4*G*), whereas IBA1 immunostaining was substantially increased in *Aire*$^{-/-}$ retinas in both mo-MΦs and microglia (Fig. 4*H*). *Lgals3* and *Aif1* are representative of the 145 genes that are up-regulated in both mo-MΦs and microglia in *Aire*$^{-/-}$ retinas. Thirty of these genes are shown in *SI Appendix*, Fig. S4*B*.

Taken together, these findings show that, although mo-MΦs and microglia express similar markers and undergo similar gene expression changes in *Aire*$^{-/-}$ retinas, they still maintain distinct transcriptional profiles.

Widespread Responses to IFN Gamma Among Resident Retinal Cells. We next examined the gene expression changes in resident retinal cell types in *Aire*$^{-/-}$ retinas. Cross-sample normalization was first performed via mean-scaling of the raw transcript copies per cell in each cell type independently. Using Monocle2 (35, 36), we generated a negative binomial regression model that included parameters for genotype, cell type, sequencing depth, and batch effects. This permitted the calculation of a z-scored genotype regression coefficient for each gene and the identification of differentially expressed genes on a per-cell type basis. To identify gene sets with differential representation in WT vs. *Aire*$^{-/-}$ datasets, genes were ranked based on the z-scored genotype regression coefficient for each gene in each cell type, and this ranking was used for a preranked Gene Set Enrichment Analysis (GSEA) (37). This preranked GSEA was performed with the Hallmark gene sets curated by the Molecular Signatures DataBase (MSigDB) (38) to identify gene sets that were enriched in *Aire*$^{-/-}$ vs. WT retinas in both grade 2 and grade 3 disease.

To examine gene expression changes that may underlie a common disease process across multiple cell types, we examined MSigDB Hallmark gene sets that were significantly enriched (q-value < 0.05) in 3 or more cell types and found multiple enriched gene sets in both grade 2 and grade 3 disease (Fig. 5 *A* and *B*). Notably, there were more enriched gene sets in grade 3 disease compared to grade 2 disease, which is consistent with the increased disease severity. Of these genes sets, the IFN-responsive gene sets appeared to be the most significantly enriched across all resident retinal cell types. As only IFN gamma, but not -alpha or -beta, transcripts were detected in the *Aire*$^{-/-}$ retina dataset, we presume that these gene expression changes were driven by IFN gamma, consistent with the predominant Th1 response. By examining the regression coefficients of IFN gamma stimulated genes as defined in the Hallmark Interferon Gamma Response gene set, we identified genes that were differentially expressed across multiple cell types, as well as those that were differentially expressed in specific cell types (Fig. 5 *C* and *D*).

One example of a gene that was significantly up-regulated across all retinal cell types is the transcription factor *Irf1*, a major target of IFN gamma signaling (*SI Appendix*, Fig. S5*A*). Additionally, expression of *Psmb9*, an IRF1 target gene, was increased in all retinal cell types (*SI Appendix*, Fig. S5*B*). PSMB9 is a subunit of the immunoproteasome, which is responsible for the processing of peptides for display by class I MHC proteins. Consistent with scRNA-seq data, immunostaining for IRF1 and PSMB9 showed widespread up-regulation in *Aire*$^{-/-}$ retinas (Fig. 5 *E* and *F*). These observations imply that resident retinal cells exhibit enhanced antigen presentation in *Aire*$^{-/-}$ retinas, thereby further stimulating the autoimmune process.

The Muller Glial Response to IFN Gamma. Although all resident retinal cell types appear to be responsive to IFN gamma, the transcript heatmaps in Fig. 5 *C* and *D* show the greatest responses in Muller glia. Consistent with this transcriptome analysis, immunostaining of *Aire*$^{-/-}$ retinas showed that IRF1 was most significantly up-regulated in Muller glia (marked by nuclear SOX9 immunostaining in the INL) (Fig. 6*A* and *SI Appendix*, S5 *A* and *E*).

Using a specificity score of ≥0.4 (Monocle2) as a threshold for Muller glia, we identified IFN gamma target genes that were up-regulated and enriched in Muller glia in *Aire*$^{-/-}$ retinas. Examples are shown in Fig. 6*B* (see also *SI Appendix*, Fig. S5 *C* and *D*). The increase in expression of known IFN gamma target genes *C4b* and *Cd274* was confirmed by fluorescent ISH (Fig. 6 *C* and *D*). *C4b* is a complement factor that promotes inflammation, as deletion of *C4b* is protective in EAU (39). *Cd274* codes for PD-L1, a checkpoint regulator that dampens the adaptive immune response and has been implicated in suppressing EAU (40). In addition, the up-regulation of *Vcam1* in Muller glia is consistent with an earlier study on EAU, which showed the up-regulation of VCAM1 in Muller glial radial processes by immunostaining (41). *Vcam1* codes for Vascular Cell Adhesion Molecule 1, a protein involved in leukocyte migration into sites of inflammation.

Interestingly, multiple MHC class II genes are preferentially up-regulated in Muller glia in *Aire*$^{-/-}$ retinas (Fig. 6*E*). These genes are typically expressed in APCs including macrophages and dendritic cells. By immunostaining, MHC class II proteins were found to be enriched in Muller glial cell bodies (marked by arrow indicating nuclear SOX9 in Fig. 6*F*) and in their radial processes (Fig. 6*F*). Some of these MHC class II+ radial processes appeared to be in direct apposition to CD4+ T cells (arrowhead in Fig. 6*F*), suggesting that Muller glia may be functioning as APCs in *Aire*$^{-/-}$ retinas.

Discussion

This paper describes the application of scRNA-seq to characterize spontaneous uveoretinitis in *Aire*$^{-/-}$ mice. Based on the abundances of different immune cell types, the patterns of gene expression in immune and retinal cells, and the results of a parallel analysis by immunostaining and ISH, we infer that 1) the dominant effector response in *Aire*$^{-/-}$ retinas is Th1-driven, 2) the development of tertiary lymphoid structures constitutes an integral part of the *Aire*$^{-/-}$ retinal phenotype, 3) a subset of monocytes convert to either a macrophage/microglia state or a dendritic cell state, 4) all major classes of resident retinal cells respond to IFN gamma as evidenced by changes in their patterns of gene expression, and 5) Muller glia up-regulate specific genes in response to IFN gamma and may act as APCs. This study adds to a growing body of evidence showing that ocular inflammation is context-specific in terms of the molecular mechanisms and immune cell types involved (5).

The dominant effector response in uveitis is known to differ among animal models. In the classical EAU model, the use of killed mycobacteria in CFA promotes a Th17-dominant response that requires IL-17 for both the induction and the progression of uveitis (42). In contrast, in the R161H transgenic mouse line, which develops spontaneous uveitis through the expression of an IRBP-specific TCR transgene, Th1 cells appear to play a central role based on the large IFN gamma response (43). The present work supports a similarly central role for Th1 cells in *Aire*$^{-/-}$ uveoretinitis based on the abundance of Th1 cells, the presence of IFN gamma transcripts, and an IFN gamma-response gene expression signature in both immune and resident retinal cell types. These findings are consistent with previous work showing

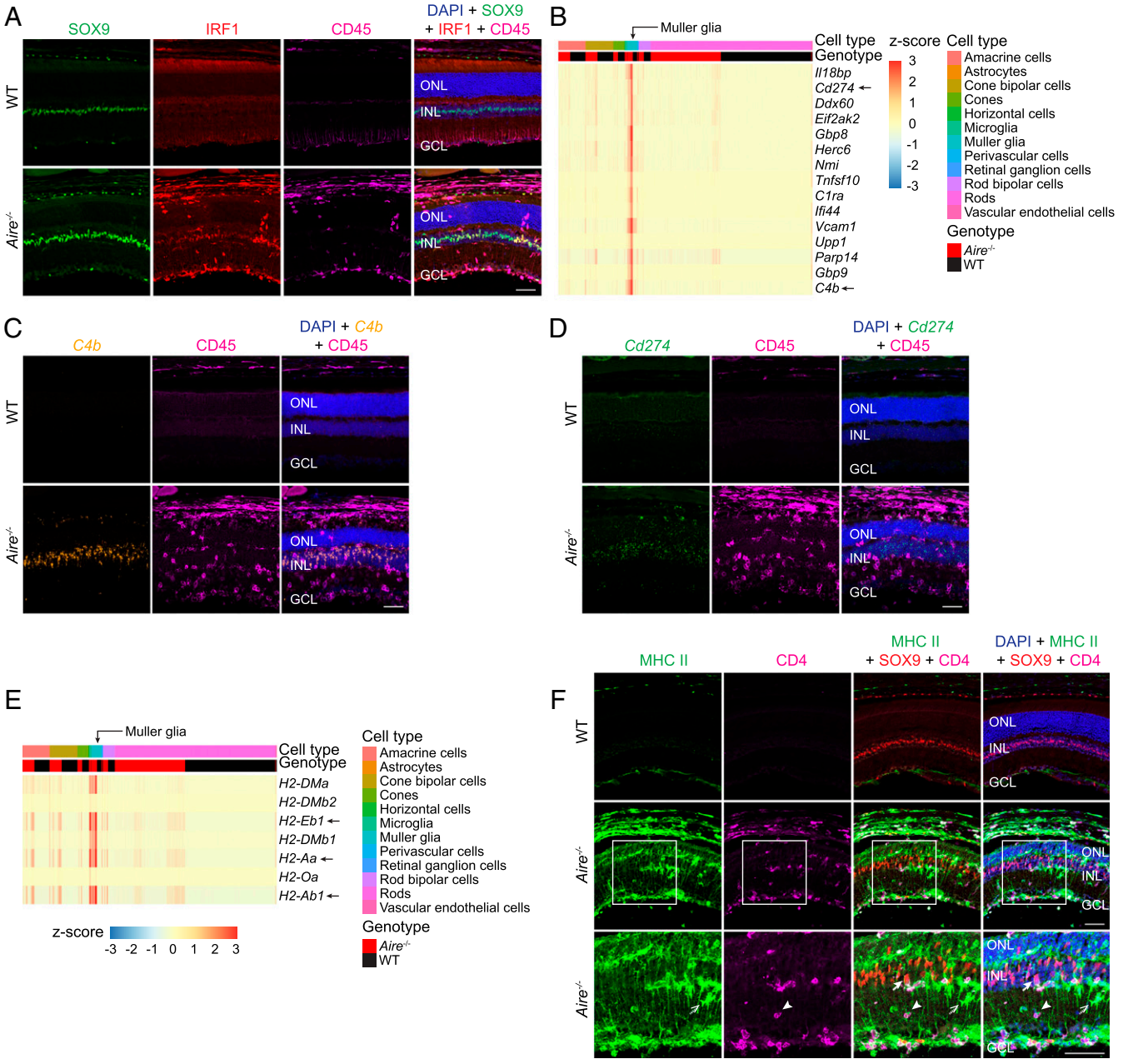

Fig. 6. Activation of IFN gamma target genes in Muller glia in *Aire*$^{-/-}$ retinas. (*A*) Immunostaining of cross-sections of WT vs. *Aire*$^{-/-}$ retinas showing SOX9 (green), IRF1 (red), CD45 (magenta), and nuclei (DAPI; blue). SOX9 marks RPE nuclei (near the top of the image), Muller glia nuclei in the INL, and astrocyte nuclei in the GCL. (*B*) Heatmap showing, by cell type, IFN gamma target genes that are preferentially up-regulated in Muller glia in *Aire*$^{-/-}$ vs. WT retinas. Individual cells are arrayed across the horizontal axis, and genes are shown along the vertical axis. Up-regulation of genes indicated by arrows was validated by fluorescent ISH in *C*. (*C*) Retinal cross-sections as in *A* showing fluorescent ISH of *C4b* transcripts (orange) and immunofluorescence of CD45 (magenta); nuclei marked by DAPI (blue). (*D*) Retinal cross-sections as in *A* showing fluorescent ISH of *Cd274* transcripts (green) and immunofluorescent staining of CD45 (magenta); nuclei are marked by DAPI (blue). (*E*) Heatmap as in *B* showing, by cell type, MHC class II genes that are significantly up-regulated in *Aire*$^{-/-}$ vs. WT retinas. MHC class II genes include the I-A and I-E alloantigens that can be detected by the anti-MHC II I-A/I-E antibody (arrows). (*F*) Retinal cross-sections as in *A* showing MHC II (I-A/I-E) (green), SOX9 (red), CD4 (magenta), and nuclei (DAPI; blue). A CD4+ T cell (indicated by arrowheads) is seen associating with an MHC class II+ process of a SOX9+ Muller glial cell (nucleus indicated by arrows). In addition, SOX9− cells with intense MHC class II staining (indicated by dashed arrows) scattered across the retina are mostly likely microglia, Mo-MΦs, or Mo-DCs. (Scale bars in *A*, *C*, *D*, and *F*, 50 μm.)

that many nonocular tissue pathologies in *Aire*$^{-/-}$ mice are Th1 dependent (19).

By immunostaining of *Aire*$^{-/-}$ retinas, we observed aggregates of T follicular helper cells, B cells, plasmablasts, plasma cells, and APCs that resemble TLSs. TLSs can be defined as unencapsulated, but structurally and functionally organized, aggregates of lymphoid cells that form in tissues other than primary lymphoid organs (i.e., thymus and bone marrow) or secondary lymphoid organs (i.e., lymph nodes, spleen, and Peyer's patches) in the context of chronic inflammation (26, 44, 45). We use the term TLSs, instead of tertiary lymphoid organs (TLOs) because we have demonstrated some but not all of the features of TLOs (44). TLO features include 1) anatomically distinct yet adjacent B and T cell compartments, 2) the presence of PNAd-positive HEVs in the

T cell compartment, and 3) the presence of germinal center reactions as evidenced by the presence of plasmablasts and plasma cells. In contrast to the diffuse inflammatory cellular infiltrates seen in the EAU model, the spatial organization of the retinal TLSs studied here more closely resembles that of lymphoid tissues. Similar TLSs have been described in the R161H transgenic mouse line (25), another model of spontaneous uveitis (described in the preceding paragraph). In R161H mice, retinas with TLSs initially have lower clinical and histological disease scores as well as slower loss of visual function (as measured by the electroretinogram) compared to retinas that lack TLSs, but the presence of well-developed, late-stage TLSs with abundant plasma cells was associated with increased visual loss and disease progression, presumably due to autoantibody production (25). Similarly, the presence of plasma cells in TLSs in *Aire*$^{-/-}$ retinas suggests that autoantibodies may also contribute to disease progression in *Aire*$^{-/-}$ uveoretinitis. There is evidence that autoantibodies play a pathogenic role in the EAU model (46) and in human uveitis (47, 48).

Retinal microglia, which arise from the yolk sac, are difficult to distinguish from mo-MΦs as the 2 cell populations share many of the same markers and both microglia and mo-MΦs up-regulate many of the same genes and can occupy new tissue niches in response to disease. A previous study that utilized irradiated mice injected with bone marrow (BM) cells marked by enhanced green fluorescent protein showed that BM-derived monocytes can populate the normal retina and assume microglial-like morphology with expression of classical microglial markers (31). The migration of BM-derived cells was enhanced in a model of *N*-methyl-*N*-nitrosourea–induced retinal injury, and the BM-derived microglial-like cells were restricted to the juxtapapillary and peripheral regions of the retina (31). More recently, fate-mapping studies in mouse models of photoreceptor injury and degeneration have shown that resident microglia migrate to the subretinal space where they adhere to the apical RPE, while mo-MΦs occupy the vacated microglial niche in the neuroretina and do not migrate to the subretinal space (29, 34). By immunostaining of *Aire*$^{-/-}$ retinas, we observed CD14- and P2ry12-positive cells (i.e., mo-MΦs) mainly in the neural retina, although some were found in the subretinal space adhering to the apical RPE. The differences across retinal disease models imply that the tissue niches occupied by microglia and mo-MΦs can vary depending on the disease context.

Our pseudotime analysis expands on this dynamic picture by implying that many monocytes transition from a state characterized by markers such as *Ccr2* and *Ly6c2* to a mo-MΦ state characterized by markers such as *Hexb and Trem2.* The rapid down-regulation of *Ccr2* in monocytes infiltrating the retina has also been described in the context of photoreceptor degeneration (49). Mo-MΦs are difficult to distinguish from resident retinal microglia as they also express conventional microglial markers such as *P2ry12* and *Tmem119*, a finding that is consistent with recent scRNA-seq studies of fluorescence-activated cell sorting-purified microglia and mo-MΦs isolated from murine retina and brain (28–30, 50). The down-regulation of genes such as *Ccr2* and the up-regulation of genes such as *Tmem119* may account for the previously observed heterogeneity in gene expression of monocyte-derived cells at early time points after these cells have infiltrated the retina in the context of light-induced photoreceptor degeneration (29, 30). The pseudotime analysis also implies that a distinct subset of monocytes transitions to a dendritic cell state characterized by markers such as *Clec9a* and *Zbtb46*. Interestingly, both the mo-MΦ and mo-DC states were associated with an up-regulation of *Smad7*, a marker of TGF-β signaling.

The scRNA-seq and ISH analyses reveal TGF-β2 expression in the INL in *Aire*$^{-/-}$ retinas. TGF-β2 has potent immunosuppressive properties (21, 51) and is thought to contribute to ocular immune privilege (5). In the context of *Aire*$^{-/-}$ uveoretinitis, TGF-β2 may mitigate against excessive immune-mediated destruction through its effects on Th1 cells and microglia/mo-MΦs. Consistent with this idea, the induction of *IL10* expression in Th1 cells has been shown to be TGF-β dependent (22), and the Th1 cells in the *Aire*$^{-/-}$ retina exhibit distinct *Cd40lg*+ and *IL10*+ states that most likely represent activated and self-regulatory states, respectively (20). Also consistent with this idea, genetic ablation of *Tgfbr2* in spinal cord mo-MΦs (32) and in retinal microglia (33) resulted in down-regulation of classical microglial markers such as *Tmem119* and conversion to a more proinflammatory phenotype.

The IFN gamma response gene expression signature that we observe in all major classes of resident retinal cells is characterized by widespread IRF1 up-regulation and up-regulation of putative IFN gamma target genes across retinal cell types. The role of IFN gamma in uveoretinitis appears to be multifaceted. Retinal production of IFN gamma, either by expression of a transgene (52) or by infusing an IRBP-specific Th1-like T cell line that produces large amounts of IFN gamma (53), appears to be uveitogenic. Moreover, disease induction in an EAU model based on injection of antigen-exposed dendritic cells requires host production of IFN gamma (54). However, removing IFN gamma, either by systemic administration of a neutralizing antibody (55) or by genetic deletion (56), exacerbated uveoretinitis in EAU instead of conferring a protective effect. These differences in the effects of IFN gamma in the context of uveoretinitis have been attributed to differences in the stage of the disease at which IFN gamma exposure occurs, with early exposure to IFN gamma eliciting an antiinflammatory effect and late exposure eliciting a proinflammatory effect (57, 58).

One intriguing instance of a cell type-specific up-regulation of putative IFN gamma target genes is the increased production of MHC class II messenger RNAs and proteins in Muller glia, with evidence of direct contact between Muller glia processes and CD4+ T cells. Muller glia are the major glial component of the retina, and their processes densely ramify throughout the entirety of the neural retina between the nerve fiber layer and the outer limiting membrane. Thus, any immune cell infiltrating the retina will come into contact with Muller glia processes. Under normal conditions, Muller glia are thought to contribute to ocular immune privilege by inhibiting the proliferation and activation of lymphocytes through a direct-contact mechanism, as demonstrated in cultured Muller glia (59). The addition of IFN gamma in vitro has been shown to induce production of MHC class II proteins in cultured Muller glia (60) and enable them to act as APCs in a MHC class II-dependent fashion to stimulate the proliferation of cocultured T cells (61). Consistent with these in vitro studies, our findings suggest that Muller glia may act as APCs in vivo in the context of *Aire*$^{-/-}$ uveoretinitis, although the relative contributions of Muller glia compared to more conventional APCs in the uveoretinitis disease process remain to be determined.

In sum, the present study demonstrates the utility of scRNA-seq as an unbiased tool for investigating immune-mediated pathogenesis in the retina, including a systematic assessment of the cell types in the inflammatory milieu and the response of the resident retinal cells to disease progression. This work suggests that scRNA-seq could be used to identify biomarkers and therapeutic targets in ocular inflammatory disorders.

Materials and Methods

All animal experiments were approved by and conducted in accordance with the regulations of the Institutional Animal Care and Use Committee at Johns Hopkins University School of Medicine (protocol MO16M367). Mouse husbandry, scRNA-seq, in situ hybridization, immunostaining, and computational methods are described in *SI Appendix*. scRNAseq data were submitted to the National Center for Biotechnology Information Gene Expression Omnibus database under accession numbers GSE132229 and GSM3854512–3854519. The annotated datasets can be viewed at https://jacobheng.shinyapps.io/uveoretinitis/ and http://loom.gofflab.org. Supplementary code for processing and visualizing the scRNA-seq data can be found in an R package, cellwrangler, available at https://github.com/jacobheng/cellwrangler.

ACKNOWLEDGMENTS. We thank David Mohr (Johns Hopkins Medical Institutions Genetic Research Core Facility) for his assistance with sequencing the scRNA-seq libraries; Melissa Olson and Kakali Sarkar for their assistance with preparing some of the scRNA-seq libraries; Peter Campochiaro for sharing his fundus imaging equipment and expertise; Daniel Saban, Jeff Mumm, Mark Soloski, Debebe Theodros, Yanshu Wang, and Chen Yu for helpful advice; and Peter Dimitrion, Mark Sabbagh, and Mark Soloski for helpful comments on the manuscript. This work was supported by the Jerome L. Greene Foundation (J.S.H and J.N.); the Thomas J. Kelly and Mary L. Kelly Young Scholar Award (to J.S.H); the Howard Hughes Medical Institute (J.W. and J.N.); the Johns Hopkins University Catalyst and Synergy Awards (L.A.G.); and the Chan-Zuckerberg Initiative Donor Advised Fund Grant 2018-183445 (to G.L.S.-O. and L.A.G.).

1. J. E. Thorne *et al*., Prevalence of noninfectious uveitis in the United States: A claims-based analysis. *JAMA Ophthalmol.* **134**, 1237–1245 (2016).
2. M. S. Suttorp-Schulten, A. Rothova, The possible impact of uveitis in blindness: A literature survey. *Br. J. Ophthalmol.* **80**, 844–848 (1996).
3. M. D. de Smet *et al*., Cellular immune responses of patients with uveitis to retinal antigens and their fragments. *Am. J. Ophthalmol.* **110**, 135–142 (1990).
4. R. R. Caspi, A look at autoimmunity and inflammation in the eye. *J. Clin. Invest.* **120**, 3073–3083 (2010).
5. V. L. Perez, R. R. Caspi, Immune mechanisms in inflammatory and degenerative eye disease. *Trends Immunol.* **36**, 354–363 (2015).
6. J. Chen *et al*., Comparative analysis of induced vs. spontaneous models of autoimmune uveitis targeting the interphotoreceptor retinoid binding protein. *PLoS One* **8**, e72161 (2013).
7. T. Lambe *et al*., Limited peripheral T cell anergy predisposes to retinal autoimmunity. *J. Immunol.* **178**, 4276–4283 (2007).
8. M. S. Anderson *et al*., Projection of an immunological self shadow within the thymus by the aire protein. *Science* **298**, 1395–1401 (2002).
9. C. E. Egwuagu, P. Charukamnoetkanok, I. Gery, Thymic expression of autoantigens correlates with resistance to autoimmune disease. *J. Immunol.* **159**, 3109–3112 (1997).
10. W. Jiang, M. S. Anderson, R. Bronson, D. Mathis, C. Benoist, Modifier loci condition autoimmunity provoked by Aire deficiency. *J. Exp. Med.* **202**, 805–815 (2005).
11. J. DeVoss *et al*., Spontaneous autoimmunity prevented by thymic expression of a single self-antigen. *J. Exp. Med.* **203**, 2727–2735 (2006). Correction in: *J. Exp. Med.* 204, 203 (2007).
12. N. Fujikado *et al*., Aire inhibits the generation of a perinatal population of interleukin-17A-producing γδ T cells to promote immunologic tolerance. *Immunity* **45**, 999–1012 (2016).
13. S. Bourgault *et al*., Retinal degeneration in autoimmune polyglandular syndrome type 1: A case series. *Br. J. Ophthalmol.* **99**, 1536–1542 (2015).
14. A. Couturier, A. P. Brézin, Ocular manifestations of autoimmune polyendocrinopathy syndrome type 1. *Curr. Opin. Ophthalmol.* **27**, 505–513 (2016).
15. J. S. Heng *et al*., Hypoxia tolerance in the Norrin-deficient retina and the chronically hypoxic brain studied at single-cell resolution. *Proc. Natl. Acad. Sci. U.S.A.* **116**, 9103–9114 (2019).
16. E. Papalexi, R. Satija, Single-cell RNA sequencing to explore immune cell heterogeneity. *Nat. Rev. Immunol.* **18**, 35–45 (2018).
17. R. K. Agarwal, P. B. Silver, R. R. Caspi, Rodent models of experimental autoimmune uveitis. *Methods Mol. Biol.* **900**, 443–469 (2012).
18. E. Becht *et al*., Dimensionality reduction for visualizing single-cell data using UMAP. *Nat. Biotechnol.* **37**, 38–44 (2018).
19. J. J. Devoss *et al*., Effector mechanisms of the autoimmune syndrome in the murine model of autoimmune polyglandular syndrome type 1. *J. Immunol.* **181**, 4072–4079 (2008).
20. G. Murugaiyan, R. Agrawal, G. C. Mishra, D. Mitra, B. Saha, Functional dichotomy in CD40 reciprocally regulates effector T cell functions. *J. Immunol.* **177**, 6642–6649 (2006).
21. S. Sanjabi, S. A. Oh, M. O. Li, Regulation of the immune response by TGF-β: From conception to autoimmunity and infection. *Cold Spring Harb. Perspect. Biol.* **9**, a022236 (2017).
22. D. J. Huss *et al*., TGF-beta enhances effector Th1 cell activation but promotes self-regulation via IL-10. *J. Immunol.* **184**, 5628–5636 (2010).
23. A. Hutloff, T follicular helper-like cells in inflamed non-lymphoid tissues. *Front. Immunol.* **9**, 1707 (2018).
24. D. A. Rao, T cells that help B cells in chronically inflamed tissues. *Front. Immunol.* **9**, 1924 (2018).
25. J. L. Kielczewski, R. Horai, Y. Jittayasothorn, C.-C. Chan, R. R. Caspi, Tertiary lymphoid tissue forms in retinas of mice with spontaneous autoimmune uveitis and has consequences on visual function. *J. Immunol.* **196**, 1013–1025 (2016).
26. E. Pipi *et al*., Tertiary lymphoid structures: Autoimmunity goes local. *Front. Immunol.* **9**, 1952 (2018).
27. A. M. Wengner *et al*., CXCR5- and CCR7-dependent lymphoid neogenesis in a murine model of chronic antigen-induced arthritis. *Arthritis Rheum.* **56**, 3271–3283 (2007).
28. M. J. C. Jordão *et al*., Single-cell profiling identifies myeloid cell subsets with distinct fates during neuroinflammation. *Science* **363**, eaat7554 (2019).
29. E. G. O'Koren *et al*., Microglial function is distinct in different anatomical locations during retinal homeostasis and degeneration. *Immunity* **50**, 723–737.e7 (2019).
30. K. E. Ronning, S. J. Karlen, E. B. Miller, M. E. Burns, Molecular profiling of resident and infiltrating mononuclear phagocytes during rapid adult retinal degeneration using single-cell RNA sequencing. *Sci. Rep.* **9**, 4858 (2019).
31. H. Kaneko, K. M. Nishiguchi, M. Nakamura, S. Kachi, H. Terasaki, Characteristics of bone marrow-derived microglia in the normal and injured retina. *Invest. Ophthalmol. Vis. Sci.* **49**, 4162–4168 (2008).
32. H. Lund *et al*., Fatal demyelinating disease is induced by monocyte-derived macrophages in the absence of TGF-β signaling. *Nat. Immunol.* **19**, 1–7 (2018).
33. W. Ma *et al*., Absence of TGFβ signaling in retinal microglia induces retinal degeneration and exacerbates choroidal neovascularization. *eLife* **8**, e42049 (2019).
34. E. G. O'Koren, R. Mathew, D. R. Saban, Fate mapping reveals that microglia and recruited monocyte-derived macrophages are definitively distinguishable by phenotype in the retina. *Sci. Rep.* **6**, 20636 (2016).
35. C. Trapnell *et al*., The dynamics and regulators of cell fate decisions are revealed by pseudotemporal ordering of single cells. *Nat. Biotechnol.* **32**, 381–386 (2014).
36. X. Qiu *et al*., Single-cell mRNA quantification and differential analysis with Census. *Nat. Methods* **14**, 309–315 (2017).
37. A. Subramanian *et al*., Gene set enrichment analysis: A knowledge-based approach for interpreting genome-wide expression profiles. *Proc. Natl. Acad. Sci. U.S.A.* **102**, 15545–15550 (2005).
38. A. Liberzon *et al*., The Molecular Signatures Database (MSigDB) hallmark gene set collection. *Cell Syst.* **1**, 417–425 (2015).
39. L. Zhang, B. A. Bell, Y. Li, R. R. Caspi, F. Lin, Complement component C4 regulates the development of experimental autoimmune uveitis through a T cell-intrinsic mechanism. *Front. Immunol.* **8**, 1116 (2017).
40. D. J. Lee, A. W. Taylor, Recovery from experimental autoimmune uveitis promotes induction of antiuveitic inducible Tregs. *J. Leukoc. Biol.* **97**, 1101–1109 (2015).
41. M. Makhoul *et al*., Characterization of retinal expression of vascular cell adhesion molecule (VCAM-1) during experimental autoimmune uveitis. *Exp. Eye Res.* **101**, 27–35 (2012).
42. D. Luger *et al*., Either a Th17 or a Th1 effector response can drive autoimmunity: Conditions of disease induction affect dominant effector category. *J. Exp. Med.* **205**, 799–810 (2008).
43. R. Horai *et al*., Spontaneous ocular autoimmunity in mice expressing a transgenic T cell receptor specific to retina: A tool to dissect mechanisms of uveitis. *Curr. Mol. Med.* **15**, 511–516 (2015).
44. K. Neyt, F. Perros, C. H. GeurtsvanKessel, H. Hammad, B. N. Lambrecht, Tertiary lymphoid organs in infection and autoimmunity. *Trends Immunol.* **33**, 297–305 (2012).
45. E. J. Colbeck, A. Ager, A. Gallimore, G. W. Jones, Tertiary lymphoid structures in cancer: Drivers of antitumor immunity, immunosuppression, or bystander sentinels in disease? *Front. Immunol.* **8**, 1830 (2017).
46. G. Pennesi *et al*., A humanized model of experimental autoimmune uveitis in HLA class II transgenic mice. *J. Clin. Invest.* **111**, 1171–1180 (2003).
47. A. Heiligenhaus, E. Miserocchi, C. Heinz, V. Gerloni, K. Kotaniemi, Treatment of severe uveitis associated with juvenile idiopathic arthritis with anti-CD20 monoclonal antibody (rituximab). *Rheumatology (Oxford)* **50**, 1390–1394 (2011).
48. J. Jiménez-Alonso *et al*., CD5+ B cells and uveitis. *Ann. Rheum. Dis.* **61**, 854–855 (2002).
49. F. Sennlaub *et al*., CCR2(+) monocytes infiltrate atrophic lesions in age-related macular disease and mediate photoreceptor degeneration in experimental subretinal inflammation in Cx3cr1 deficient mice. *EMBO Mol. Med.* **5**, 1775–1793 (2013).
50. T. R. Hammond *et al*., Single-cell RNA sequencing of microglia throughout the mouse lifespan and in the injured brain reveals complex cell-state changes. *Immunity* **50**, 253–271.e6 (2019).
51. R. A. Flavell, S. Sanjabi, S. H. Wrzesinski, P. Licona-Limón, The polarization of immune cells in the tumour environment by TGFbeta. *Nat. Rev. Immunol.* **10**, 554–567 (2010).
52. K. Geiger *et al*., Transgenic mice expressing IFN-gamma in the retina develop inflammation of the eye and photoreceptor loss. *Invest. Ophthalmol. Vis. Sci.* **35**, 2667–2681 (1994).
53. H. Xu, L. V. Rizzo, P. B. Silver, R. R. Caspi, Uveitogenicity is associated with a Th1-like lymphokine profile: Cytokine-dependent modulation of early and committed effector T cells in experimental autoimmune uveitis. *Cell. Immunol.* **178**, 69–78 (1997).
54. J. Tang *et al*., Autoimmune uveitis elicited with antigen-pulsed dendritic cells has a distinct clinical signature and is driven by unique effector mechanisms: Initial encounter with autoantigen defines disease phenotype. *J. Immunol.* **178**, 5578–5587 (2007).
55. R. R. Caspi *et al*., Endogenous systemic IFN-gamma has a protective role against ocular autoimmunity in mice. *J. Immunol.* **152**, 890–899 (1994).
56. L. S. Jones *et al*., IFN-gamma-deficient mice develop experimental autoimmune uveitis in the context of a deviant effector response. *J. Immunol.* **158**, 5997–6005 (1997).
57. T. K. Tarrant *et al*., Interleukin 12 protects from a T helper type 1-mediated autoimmune disease, experimental autoimmune uveitis, through a mechanism involving interferon γ, nitric oxide, and apoptosis. *J. Exp. Med.* **189**, 219–230 (1999).
58. R. S. Grajewski *et al*., Activation of invariant NKT cells ameliorates experimental ocular autoimmunity by a mechanism involving innate IFN-γ production and dampening of the adaptive Th1 and Th17 responses. *J. Immunol.* **181**, 4791–4797 (2008).
59. R. R. Caspi, F. G. Roberge, R. B. Nussenblatt, Organ-resident, nonlymphoid cells suppress proliferation of autoimmune T-helper lymphocytes. *Science* **237**, 1029–1032 (1987).
60. T. Mano, N. Tokuda, D. G. Puro, Interferon-gamma induces the expression of major histocompatibility antigens by human retinal glial cells. *Exp. Eye Res.* **53**, 603–607 (1991).
61. F. G. Roberge, R. R. Caspi, R. B. Nussenblatt, Glial retinal Müller cells produce IL-1 activity and have a dual effect on autoimmune T helper lymphocytes. Antigen presentation manifested after removal of suppressive activity. *J. Immunol.* **140**, 2193–2196 (1988).